Original Article

Computer-aided rational design of acyclovir analogs to inhibit purine nucleoside phosphorylase

Nusrat Jahan Selsi[1], Lira Barua[2], Debpriya Bhattacharjee[1], Gulamur Rahman[1], Syeda Sakiatuz Zannat[3], Najia Absar Munia[4], Rubaiyat Fahad[1], Tanjiba Harun Bipasha[1], Azizur Rahman[5], Raju Dash[6*]

[1]Department of Pharmacy, University of Science and Technology Chittagong, Bangladesh
[2]Department of Chemistry, University of Chittagong, Chittagong, Bangladesh
[3]Department of Physics, Astronomy and Mathematics, Faculty of Science and Technology University of Central Lancashire, Lancashire, United Kingdom
[4]Department of Pharmacy, BGC Trust University Bangladesh, Chandanaish, Bangladesh
[5]Department of Pharmacy, Southern University Bangladesh, Chittagong, Bangladesh
[6]Department of Anatomy, Dongguk University Graduate School of Medicine, Gyeongju, Korea

ARTICLE INFO

ABSTRACT

Purine nucleoside phosphorylase (PNP) is one of the major enzymes in the purine salvage pathway. It is responsible for the elevation of deoxyguanosine, and thus considered as the potent target in T-cell lymphoma. The present study examined acyclovir, reported as a low-affinity PNP inhibitor, for the rational design of new acyclovir derivatives by incorporating halogens, hydroxyl, and bulky amino groups. The molecular actions of designed derivatives were investigated by employing density functional theory, molecular docking, and binding energy calculations. The results revealed that the newly designed compounds were highly stable and showed more affinity to PNP than the parent compound, acyclovir. The quantum mechanics and molecular docking studies suggested that modification of side chains with bulky polar groups provided better binding affinities than substitutions with halogens. The resultant derivatives have strong polar interactions like His257 and Tyr88. Furthermore, the designed derivatives were within the ideal range of ADMET (absorption, distribution, metabolism, elimination, and toxicity) analysis. Considering that, these findings recommend further validation of designed acyclovir derivatives in wet lab confirmatory analysis with the emphasis on the further improvements in the treatment of T-cell-mediated diseases.

Introduction

The immune system consists of T-lymphocytes and B-lymphocytes, which fight against the bacteria and viruses that induced infection within the human body. However, overexpression of the immune system may develop malignancy (1). Uncontrolled T-cell proliferation may lead to the development of T-cell leukemia, cutaneous T-cell lymphoma, and some autoimmune diseases like rheumatoid arthritis (2, 3), psoriasis (4, 5), lupus erythematosus, and Crohn's disease.

Purine nucleoside phosphorylase (PNP) is a significant enzyme in purine salvage pathway (6), and absence of this enzyme results in T-cell (cellular immunity)-induced immune deficiency (7), although B-cell function (humoral immunity) remains unaffected. PNP deficient patients experience a rare autosomal disease with T-cell regulated immunodeficiency (8). Selective inhibition of PNP elevates the concentration of deoxyguanosine (dGuo), which sequentially phosphorylates to 2`-deoxyguanosine monophosphate (dGMP) and deoxyguanosine triphosphate (dGTP). Accumulation of dGTP inhibits ribonucleoside diphosphate reductase (9, 10) that shuts off DNA synthesis and results in T-cell apoptosis. Thus targeting PNP is a unique way to design PNP inhibitors (11, 12) and treats the patients with T-cell leukemia or experiencing tissue rejection due to organ transplantation (as PNP inhibitors are sensitive to T cells only) (7, 9).

Acyclovir is a nucleoside analog of guanosine and a human PNP inhibitor (13). Acyclovir and its metabolites are independent of PNP regulated metabolism. However, acyclovir has a Ki value of 90 μM that indicates its poor bonding with the enzyme and provides weak inhibitory activity (14). To prove the therapeutic value of PNP inhibition in T-cell lymphoma, a preliminary step is to design potent and selective inhibitors of PNP, which is considered in the present study. The strong binding between ligand and protein is usually mediated by various non-bonded interactions, which are poorly understood by classical MM force fields. Instead, Ab Initio, the application of first principles quantum mechanical (QM) calculation, provides a more accurate understanding of protein-ligand interactions compared to the classical mechanics (15). The calculation of protein-ligand binding energy by conjugating molecular mechanics calculations and continuum solvation models has been successfully applied to various protein-ligand systems for assessing the correct binding poses and ranking of the binding affinities of a series of ligands (16). Besides the binding energy and quantum mechanics

calculations, the present study employed the rational approaches to design newer acyclovir analogs with better PNP inhibitory activity. Furthermore, the designed analogs were characterized to analyze their pharmacokinetic properties.

Materials and methods

Receptor Preparation

The crystal structure of the human PNP bound with acyclovir was obtained from the Protein data bank with a PDB ID 1PWY (17). Water molecules and hetero atoms were removed from the structure, and then polar hydrogens were added to reconstruct the structure. Next, the modified structure underwent protonation to fix the dihedral angles at an environment of pH 7, 0.15 M salt concentration, and a temperature of 300 K. The solvation system was fixed with 1 dielectric constant. Considering van der Waals forces, the cut-off value was considered 10 Å. Amber 10 force field (18) with 0.05 gradient was selected to level up the atoms within the protein structure. This action is required for molecular energy function, and to speed up the ligand designing procedure. Amber 10 is one of the most popular and reliable force fields (FF) to reproduce the behavior of peptides and proteins both in the gas phase and in condensed phase that has parameters for all common amino acids (19-21). Furthermore, an electrostatic map was generated to recognize the classical residues important for hydrophobic as well as hydrogen bonds in the binding pocket of human PNP.

Design of Newer Analogs

Chemdraw is a tool used to draw the 2D structure of the molecules which can also convert 2D into 3D structure followed by geometry optimization with Becke's exchange functional combining with Lee, Yang, and Parr's (LYP) correlation functional (22-24) (B3LYP) theory, i.e., density functional theory. In these calculations, the Slater-type orbital (STO) basis was set with single polarization, and STO-3G$^+$ was incorporated (25, 26) by Jaguar Quantum Chemistry Software (27-30). To understand the effect of substitution in the molecular geometry, HOMO (highest occupied molecular orbital energy), LUMO (lowest unoccupied molecular orbital energy), and HOMO-LUMO gap were calculated for each designed compound (33).

Molecular Docking analysis

The designed compounds were initially docked to the PNP binding pocket to elucidate the binding patterns and intermolecular interactions. Molecular docking simulation was performed using the MOE 2015.10 software with the force field of Amber10: EHT (all-atom force field combining Amber 10 and 2D Extended Hueckel Theory). Also, MOE-Dock program embedded in MOE2014 was used for docking. The whole structure of each enzyme was used as a receptor to find the potential binding sites. Here the compounds were placed using

Triangle Matcher. The London dG (which estimates the free energy of ligand binding) was used as the first scoring function, which generates poses by aligning ligand triplets of atoms on triplets of α-spheres represented in receptor site points. A random triplet of α-sphere centers was used to determine the pose during each iteration. The generated pose was rescored using the London dG scoring function (31). After that, GBVI/WSA (generalized-born volume integral/weighted surface area) was used as the second scoring function, where the best conformation was saved as the output result. Also, the hits were ranked by the scoring functions, including cluster diversity and visual inspection. In addition to that, binding free energy calculation was incorporated by using the scoring function of MM/GBVI. The generalized Born/volume integral (GB/VI) implicit solvent method was used to determine the binding affinities of the potential ligands, using the force field of Amber10: EHT with R-Field solvation (32-34).

Absorption, Distribution, Metabolism, Elimination and Toxicity Prediction

ADMET (absorption, distribution, metabolism, elimination, and toxicity) analysis was carried out to predict both the physicochemical and pharmacokinetic properties of new acyclovir analogs. Availability of the wide range of online tools and software programs make it easier to evaluate these properties (35, 36). AdmetSAR (37), another online tool, was used in this study to screen the pharmacokinetic and pharmacodynamic properties of the developed acyclovir analogs.

Results

Rational designing of Acyclovir Analogs

As described above, acyclovir is a weak PNP inhibitor with a higher Ki value. Several efforts have already made to develop acyclovir derivatives like hydroxy-acyclovir, amino-acyclovir, N-aza-acyclovir, 9-(~-hydroxybutyl) guanine (carba-acyclovir), acyclovir-monophosphate, acyclovir-diphosphate, and acyclovir-triphosphate. They were designed through incorporation or extension of the side chain length, to produce variable inhibitory activities against PNP (38, 39). Among those, acyclovir-diphosphate was considered as the best PNP inhibitor because of its extraordinary Ki value of 0.0087 µM. However, it was excluded during *in vivo* analysis because of its problematic metabolic function and improper cell membrane transportation (38). In a closer look at the crystal structure of acyclovir-PNP complex, the binding site of inhibitors are located near the C-terminal region of the 6-stranded β-sheet, where the overall PNP structure is composed of an α/β-fold, consisting of a 4-stranded β-sheet, 8 α-helices, and a distorted β-barrel formed out of a 6-stranded β-sheet (Figure 1a) (40). Earlier reports revealed that the inhibitor-containing purine base interacted with purine binding hydrophobic residues of PNP. It consisted of Phe200, Val217, Met219, Val245, and
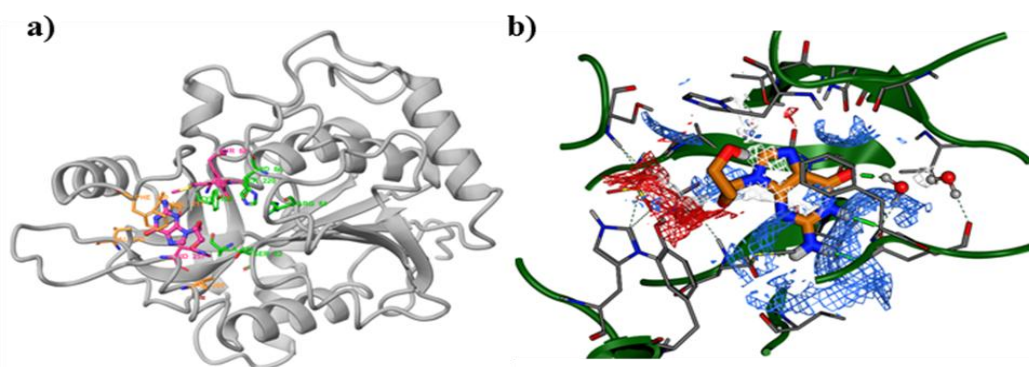
Figure 1 Binding site architecture of purine nucleoside phosphorylase in three-dimensional structure describing the presence of hydrophobic residues (orange color), anionic site residues (green color) and ribocationic mimics interacting residues (pink color) in the binding pocket of PNP (a). Electrostatic map in the active site of PNP represents the locations for hydrophobic entities as well as hydrogen bond donors and acceptors. Here, the blue color represents H-bond donor, red H-bond acceptor, and the white-gray hydrophobic region.

Val260, shown in Figure 1a (residue marked as orange color). Conversely, the adjacent subunit involved in the interactions with ribocation mimics is surrounded by Phe159, His257, Tyr88, and Met219 that are important for the catalysis by positioning the 5′-ribosyl oxygen of substrate near the 4′-ribosyl hydroxyl group that in turn is near the phosphate nucleophile, especially His257 (41). Besides, the anionic phosphate-binding site is located in line with the side chain residues of Arg84, His86, Ser220, Ala116, Ser33, Tyr192 interacting through a structural water molecule. However, the intermolecular interaction analysis of acyclovir-PNP complex revealed that the complex lacked interactions with the ribocation mimics interacting residues as well as the purine binding hydrophobic residues, which showed only hydrogen bonding and the salt bridge interactions only with Glu201 and Asn243 residues. Based on the structure based analysis between different ligands and PNP, it was found that the ether moiety present in the side chain has no impact on binding affinity and Glu and Asn at the position of 201 and 243 are crucial for effective binding in the PNP active site (17, 42-45). Initially, an electrostatic map is generated around the ligand binding site to investigate the space in the active site to elaborate the ligand, i.e., from either end (Figure 1b). The region that was localized in front of acyclovir side chain served as major H-bond accepting and donating region in the active site of PNP. Previous studies on all four generation PNP inhibitors showed that the hydrogen bonding from side chain containing hydroxyl groups of the inhibitors with the ribocationic mimics interacting residues were important for tight binding with PNP (46). Based on the unoccupied space, two modification sites at acyclovir were considered for the designing of new analogs, which might facilitate the interactions of ligand to these residues. Therefore, ten different acyclovir analogs were designed by introducing halogens, hydroxyls, and nitrogen-containing bulky groups to manipulate electronegativity and length of the side chain, to obtain proper compactness and to maximize polar interactionto the active site residues of

PNP. These groups were introduced at the eighth position of acyclovir, and its 2-hydroxyethoxymethyl side chain was thoroughly modified (Figure 2), as modifications of this chain showed significant role in inhibitory action against PNP, according to previous study (17). After that, the synthetic feasibilities of these compounds were also assessed (Table 1), where all designed compound showed synthetic feasibilities within the range of 40% to 60%.
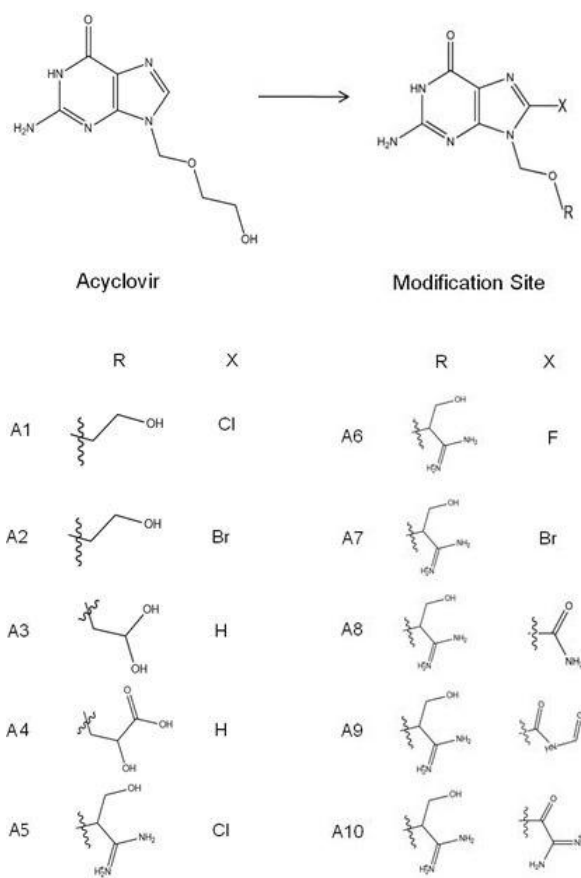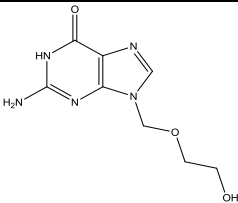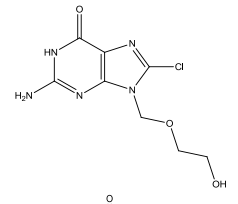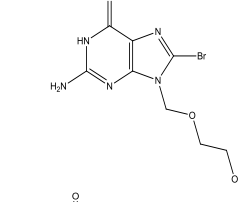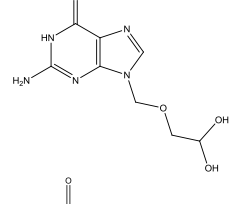

Figure 2 List of structurally-modified ten acyclovir analogs through the incorporation of halogen.

Table 1 List of new acyclovir analogs with their IUPAC name, physical characteristics, and synthesis feasibility.

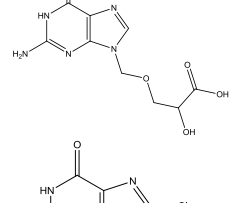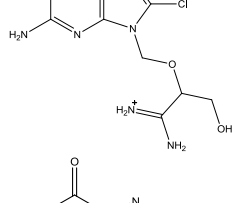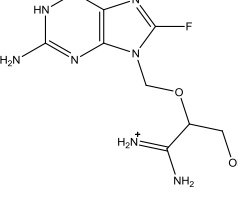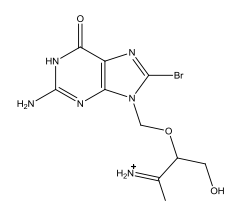| Compound Name	Structure	IUPAC Name	Molecular Weight (g/mol)	TPSA	LogP	Synthesis Feasibility, %
Acyclovir		2-Amino-9-(2-hydroxyethoxymethyl)-1H-purin-6-one	225.21	114.76	-1.19	56.25
A1		2-Amino-8-chloro-9-((2-hydroxyethoxy)methyl)-1H-purin-6(9H)-one	259.65	114.76	-0.54	58.82
A2		2-Amino-8-bromo-9-((2-hydroxyethoxy)methyl)-1H-purin-6(9H)-one	304.10	114.76	-0.43	58.82
A3		2-Amino-9-((2,2-dihydroxyethoxy)methyl)-1H-purin-6(9H)-one	241.21	134.99	-1.88	58.82
A4		3-((2-Amino-6-oxo-1H-purin-9(6H)-yl)methoxy)-2-hydroxypropanoic acid	269.22	152.06	-1.74	42.11
A5		1-Amino-2-((2-amino-8-chloro-6-oxo-1H-purin-9(6H)-yl)methoxy)-3-hydroxypropan-1-iminium	302.70	166.37	-3.06	55.00
A6		1-Amino-2-((2-amino-8-fluoro-6-oxo-1H-purin-9(6H)-yl)methoxy)-3-hydroxypropan-1-iminium	286.25	166.37	-3.57	55.00
A7		1-Amino-2-((2-amino-8-bromo-6-oxo-1H-purin-9(6H)-yl)methoxy)-3-hydroxypropan-1-iminium	347.15	166.37	-2.95	55.00

Abbreviation: TPSA = Topological polar surface area.

A8		1-Amino-2-((2-amino-8-carbamoyl-6-oxo-1H-purin-9(6H)-yl)methoxy)-3-hydroxypropan-1-iminium	311.28	209.46	-4.61	50.00
A9		1-Amino-2-((2-amino-8-(formylcarbamoyl)-6-oxo-1H-purin-9(6H)-yl)methoxy)-3-hydroxypropan-1-iminium	339.29	212.54	-4.82	45.83
A10		1-Amino-2-((2-amino-8-(2-amino-2-iminioacetyl)-6-oxo-1H-purin-9(6H)-yl)methoxy)-3-hydroxypropan-1-iminium	339.32	235.05	-6.41	50.00

Quantum Mechanical Analysis

The quantum mechanical calculation, followed by DFT optimization were applied to the designed compounds in order to represent the ionization potential, electron efficiency, electron negativity, electron excitation energy, and the hardness of the compounds in terms of highest occupied molecular orbital (HOMO) and lowest unoccupied molecular orbital energies (LUMO). High-density HOMO orbital facilitates the electrophilic attack, i.e., they can attack electron-rich regions as they lack electrons. On the other hand, when LUMO orbital is densified, it speeds up nucleophilic attack i.e., they are crowded with a negative charge and get attracted towards the positive environment (47). The difference between the energies of these two orbital is known as HOMO-LUMO gap that indicates the stability pattern and strength of electron transfer during the bond formation (28, 34, 48, 49). The lowest difference shows the highest potency of a molecule to undergo any reaction because lower energy is required to transfer the electron from the exterior orbital (50). Figure 3 shows the charge distribution in the HOMO and LUMO orbital in acyclovir and its analogs. The range of the HOMO-LUMO gap of these new ten analogs fluctuates from 0.02539 to 0.19817 eV. All of these analogs showed lower HOMO-LUMO gap compared to the acyclovir that is indicative of their better reactivity than acyclovir itself (Table 2). Among these compounds, the A4 showed the lowest gap score and A3 is the highest. As represented in Figure 3, the purine ring in the acyclovir serves only for the electrophilic and nucleophilic reactive state, which was also similar to the halogen modified A1 and A2 compounds. However, modification of the side chain with a 1-amino-3-hydroxypropyl-1-iminium group in A5 increases the nucleophilic attacking capacity of the compound, while substitution by 2-hydroxypropyl-oic acid provides a highly electrophilic surface of the compound. On the other hand, replacing hydrogen atoms by methylamide and another bulky polar group carboxamide (Figure 3) improved the electrophilicity in the side chains of A8 and A9, but in case of A10, nucleophilic attacking capacity was extremely improved due to the addition of 1-amino-2-oxoethyliminium group in the modified C8 region by replacing hydrogen. To reveal the changes in binding affinity and the interactions by acyclovir analogs, molecular docking and binding energy calculations were incorporated and discussed in further section.

Molecular Docking Interactions

Molecular docking is a bioinformatics analysis of rational drug design and discovery (51). Here docking analysis was conducted to understand the interaction patterns and binding affinity of the designed acyclovir analogs towards the PNP. The accuracy of docking protocol was validated by re-docking of a reference co-crystal ligand, where the ligand was first separated and re-docked using described docking protocol. The conformation of docked ligand was compared with the crystal structure, and the RMSD was calculated. The docking simulation produced almost similar orientation of ligand conformation like a native one with an RMSD of 0.88 Å (Figure 4). Since the lower RMSD defines a high level of the accuracy of docking protocol, it was considered further to run docking simulation. The binding affinity was predicted through docking score; the acyclovir itself obtained a docking score of -6.63 kcal/mol, whereas the score varied from -8.11 to -9.94 kcal/mol for the modified analogs. The A8, A9, and A10 analogs showed the maximum scores of -9.57, -9.84, and -9.94 kcal/mol, respectively. Furthermore, binding energy calculation revealed that the modified A8, A9, and A10 produced the highest binding energy of -71.57, -76.19, and -77.53 kcal/mol, respectively; nevertheless, the acyclovir

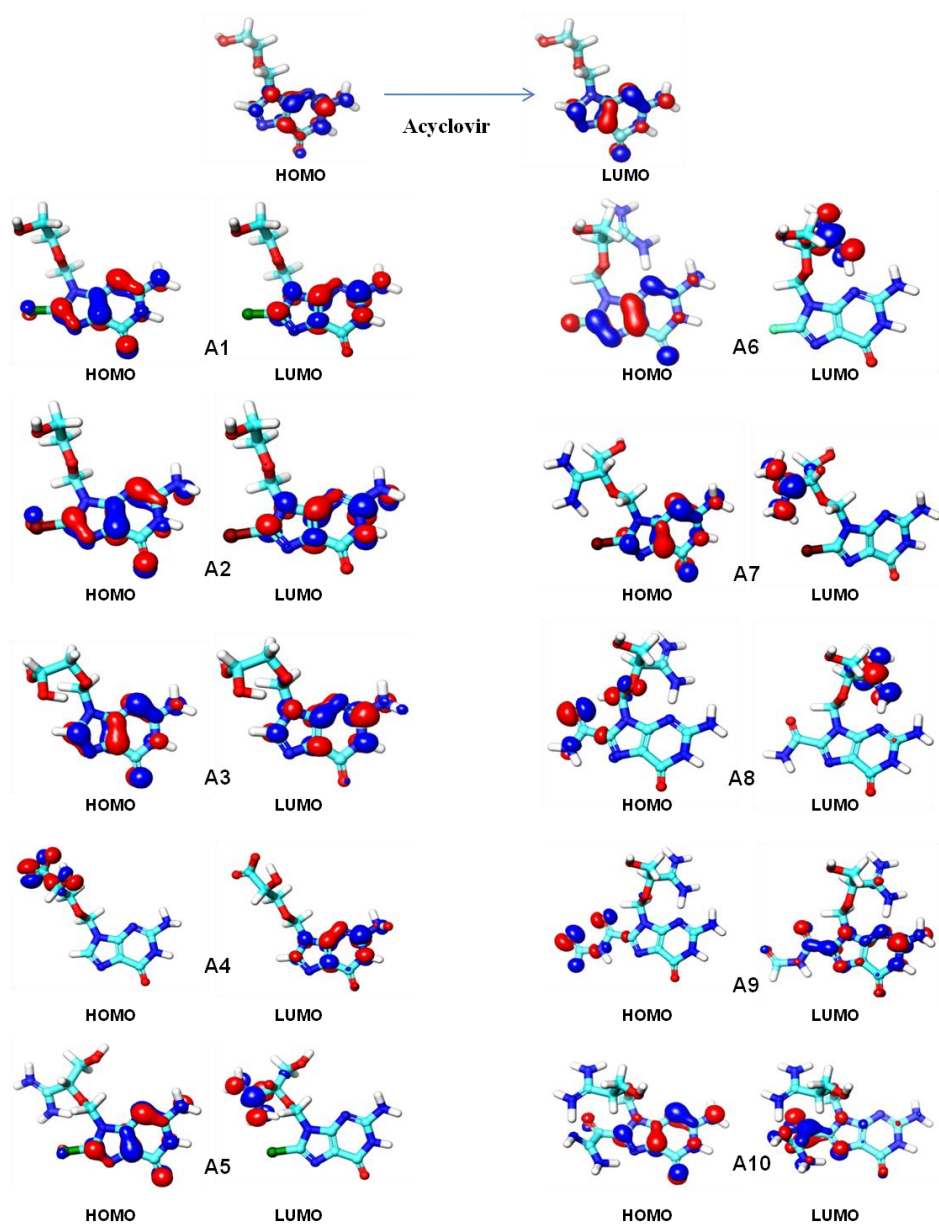**Figure 3** Representation of the localizations of HOMO and LUMO energies in designed compounds. Red color indicates positive charge and blue denotes negative charge.
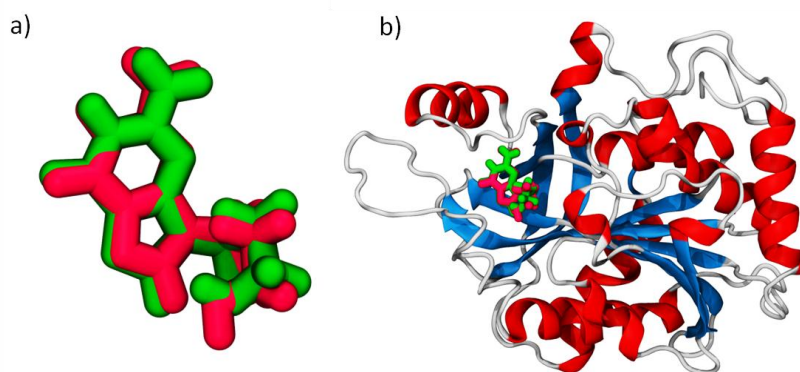

Figure 4 Predicted pose from molecular docking analysis representing the superimposed view of docked (red color) and co-crystallized native ligand (green color) in closed view of stick model (a) and within the active site of PNP (b).

showed only binding energy of -39.63 kcal/mol. These results conclude that the interactions among the modified analogs, including A8, A9, and A10 with the receptor are more spontaneous than those with the acyclovir. To gain insights into the binding mechanisms of the designed analogs, the detailed intermolecular interactions were analyzed and represented in Table 3. As seen in the Table, modification in acyclovir increased the hydrogen bonding capacity of the compounds as revealed in the QM analysis. The substitution of halogen atom at the eighth position, including chlorine and bromine induced hydrogen bonding with Ser199 and Met219 residues; however, bromine substitution made the compound to interact with His257, an important ribocation mimics interacting residue. On the other hand, 2-hydroxy ethoxy methyl side chain modified compounds; A3 and A4 made important hydrogen bonds with Tyr88 and Met219 residues. Similarly, the compounds modified with halogen atoms and 1-amino-3-hydroxypropyl-1-iminium group, i.e., A5 to A7 showed the diverse hydrogen bonding, including the interactions with His257. The highest best docking score containing compounds, i.e., A8 and A10 formed hydrogen bonds with Try88 but A10 showed this action only for His257. Comparatively, maximum polar interactions with receptor were observed in A10 compound, where it formed hydrogen bonds with Tyr88, Gly218, Asn243, His257, Ser199, and Glu259 residues.

Table 2 Results of quantum mechanics simulation, including gas-phase energy, HOMO, LUMO and HOMO-LUMO gap of acyclovir and its newly designed ten analogs.

Compound Name	Gas-Phase Energy	HOMO (eV)	LUMO (eV)	HOMO-LUMO (eV)
Acyclovir	-800.346254	-0.11501	0.08316	0.19817
A1	-1254.92794	-0.12215	0.07098	0.19313
A2	-3346.499843	-0.11978	0.07321	0.19299
A3	-874.498227	-0.1278	0.06706	0.19486
A4	-985.645764	0.12167	0.14706	0.02539
A5	-1402.261499	-0.22547	-0.12151	0.10396
A6	-1045.477292	-0.2567	-0.08587	0.17083
A7	-3493.830075	-0.22346	-0.13431	0.08915
A8	-1114.133375	-0.24807	-0.07999	0.16808
A9	-1225.936316	-0.23888	-0.08501	0.15387
A10	-1206.383526	-0.24429	-0.12646	0.11783

Abbreviation: HOMO = Highest Occupied Molecular Orbital, LUMO = Lowest Unoccupied Molecular Orbital

The interaction pattern was maximum in A10 case (Figure 5b), due to the presence of an extra amino group and nitrenium ion in the C8 modified region. This modification thus increased the binding affinity and energy of the compound to PNP, enabling the polar interactions with ribocation mimics interacting residues, including Tyr88 and His257 within the PNP binding pocket.
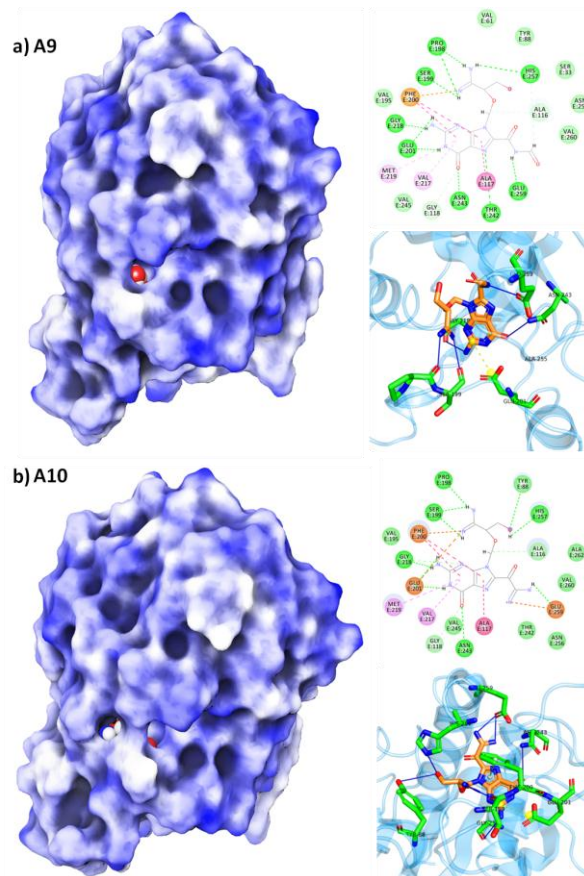

Figure 5 Binding pose of two best hits, including A9 (a) and A10 (b) obtained from the docking analysis. In each panel, the cartoon stick model of the complex is represented with 2D interaction diagram. In cartoon stick model representations, the dark blue line indicates hydrogen bonding. Also, the yellow dotted line is for pi-cation interaction. In addition, the green line between ligand and residue in 2D interaction diagram denotes hydrogen bonding, pink as hydrophobic and yellow as salt bridged and pi-cation interaction.

Absorption, Distribution, Metabolism, Elimination, and Toxicity Analysis
AdmetSAR tool was used to characterize the bioavailability and pharmacological properties (52) of the developed acyclovir analogs. Table 4 presents important parameters like permeability through the blood-brain barrier (BBB), intestinal absorption, inhibition of P-glycoprotein, CYP 2C9, human ether a-go-go related gene, oral toxicity level and also toxicity in rat. Apart from neuroactive drugs, other drugs are restricted

Table 3 List of acyclovir and their analogs with their docking score, binding energy, and residues involved in non-bonded intermolecular interactions

Compound	Binding Affinity (Kcal/mol)	Binding Energy (Kcal/mol)	Hydrogen Bonds	π-Cation Interactions	Salt Bridges
Acyclovir	-6.63	-39.63	Thr242 (2.73 Å), Asn243 (1.91 Å)	Phe200 (4.29 Å)	Glu201 (3.47Å)
A1	-8.11	-56.11	Ser199 (2.42 Å), Met219 (2.13 Å), Thr242 (3.06 Å), Asn243 (2.01 Å)	Phe200 (4.15Å)	Glu201 (3.53Å)
A2	-8.30	-56.84	Ser33(3.30Å),Ser199 (2.47 Å), Met219 (2.21 Å), Thr242 (3.25Å), Asn243 (1.87 Å), His257 (1.96 Å), Glu259 (3.34 Å)	Phe200 (4.21Å)	Glu201 (3.52Å)
A3	-7.79	-50.09	Tyr88 (1.91Å), Met 219 (2.18 Å), Thr242 (2.84 Å), Asn243 (1.84 Å)	----	Glu201 (3.39Å)
A4	-7.15	-49.05	Tyr88 (2.43Å), Tyr88 (1.76Å), Met219 (2.56Å), Thr242 (2.74 Å), Asn243 (1.88Å)	Phe200 (5.19Å)	His86 (4.99Å), Glu201 (3.41Å)
A5	-8.44	-62.00	Gly118 (3.35Å), Pro198 (1.91Å), Ser199 (1.73Å), Gly218 (2.71Å), Thr242 (2.29Å), Asn243 (1.90Å), His257 (2.03Å)	Phe200 (4.97Å)	Glu201 (3.48Å)
A6	-8.62	-64.16	Ser199 (1.79Å), Gly218 (2.78Å), Thr242 (2.88 Å), ASN243 (2.04 Å), His257 (2.27 Å), His257 (1.98 Å)	----	Glu201 (3.49Å)
A7	-8.51	-60.47	Pro198(1.81Å), Ser 199(1.75Å),Gly218 (2.32Å), His257 (1.98Å)	Phe200 (4.69Å)	Glu201 (3.49Å)
A8	-9.57	-71.93	Tyr88 (2.08 Å), Pro198(1.83Å), Ser199(1.77Å), Gly218(2.27Å), Met219 (3.67Å), Thr242 (1.88Å), Asn243 (2.09Å)	Phe200 (4.80Å)	Glu201 (3.43Å)
A9	-9.84	-76.19	Pro198 (1.78Å), Ser199 (1.76Å), Gly218 (2.35Å), Asn243 (1.95Å), Glu259 (2.44Å), Glu259 (1.77Å)	Phe200 (4.80Å)	Glu201 (3.49Å)
A10	-9.94	-77.53	Tyr88 (3.39Å), Ser199 (2.10Å), Ser199 (1.74Å), Gly218 (2.32 Å), Asn243 (2.46Å), His257 (2.00 Å), Glu259 (1.72 Å), Glu259 (1.75 Å)	Phe200 (4.80Å)	Glu201 (3.48Å)

to cross the BBB to avoid possible CNS side effects (53). In case of absorption through the BBB and intestine, these acyclovir analogs showed positive results which indicated that all compounds have better absorption capacity in the peripheral part of the body without showing any side effects because of their restrictions to cross the BBB. Again, these compounds are not inhibitory to P-glycoprotein and CYP2C9 metabolic enzyme. Nearly half of the total drug candidates are metabolized through this enzyme, which is abundant in liver and small intestine (54). As they are non-inhibitory to these enzymes, their metabolic function would not be interrupted. They are also predicted as non-inhibitor to human ether-a-go-go-related gene; most importantly, this gene is a calcium channel and blockage of this channel by any drug leads to cardiac arrhythmia (55). These ten acyclovir analogs showed similar oral toxicity, but their LD_{50} values fluctuated from 0.885 to 2.173 kg/mol. The A2 analog showed the maximum, while A3 obtained minimum LD_{50} value.

Table 4 ADMET (absorption, distribution, metabolism, elimination, and toxicity) properties of designed acyclovir based analogs were calculated from AdmetSAR server

Parameters	Acyclovir	A1	A2	A3	A4	A5	A6	A7	A8	A9	A10
Blood-brain barrier	+ (0.98)	+ (0.97)	+ (0.98)	+ (0.98)	+ (0.97)	+ (0.97)	+ (0.97)	+ (0.98)	+ (0.98)	+ (0.98)	+ (0.98)
Human intestinal absorption	+ (0.98)	+ (0.96)	+ (0.94)	+ (0.95)	+ (0.87)	+ (0.85)	+ (0.85)	+ (0.82)	+ (0.79)	+ (0.81)	+ (0.78)
P-glycoprotein inhibitor	- (0.83)	- (0.95)	- (0.95)	- (0.96)	- (0.96)	- (0.91)	- (0.93)	- (0.92)	- (0.89)	- (0.82)	- (0.83)
CYP 2C9 inhibition	- (0.86)	- (0.76)	- (0.77)	- (0.89)	- (0.88)	- (0.81)	- (0.80)	- (0.80)	- (0.87)	- (0.89)	- (0.87)
Human ether-a-go-go inhibition	- (0.89)	- (0.53)	- (0.48)	- (0.53)	- (0.69)	- (0.53)	- (0.50)	- (0.43)	- (0.52)	- (0.57)	- (0.59)
Acute oral toxicity	III (0.47)	III (0.59)	III (0.59)	III (0.57)	III (0.59)	III (0.58)	III (0.58)	III (0.58)	III (0.57)	III (0.57)	III (0.57)
Rat acute toxicity (LD$_{50}$, kg/mol)	1.52	2.04	2.17	0.88	1.61	1.47	1.65	1.68	1.00	1.76	1.296

Discussion

Earlier reports demonstrated that complete or more than 95% of PNP inhibition is necessary for increasing dGuo concentration to adequate level not only for T-cell toxicity (56), but also for other treatments including T-cell-mediated autoimmune diseases like as rheumatoid arthritis and chronicpsoriasis, transplantation of an organ, and also auto immunogenic insulin-dependent diabetes (57-59). Although several inhibitors designed based on nucleoside analogues like acyclovir have been discovered so far, these inhibitors were proved to be inefficient to inhibit PNP adequately to suppress T-cell by increasing plasma dGuo (60). It has been proposed that designing inhibitors based on the transition state mimics interacting site that could be capable to bind more strongly and with superior fidelity (56, 61). Therefore, based on the untenanted electro-potential space in the active site, ten potential compounds were designed in this study with the concern of elevated interactions with ribocation mimics interacting residues, including Phe159, His257, Tyr88, and Met219. All compounds showed moderate synthetic feasibility score, which indicates the designed compounds may not pose problems and can be easily synthesized. Synthetic feasibility scores describe that the molecule is very likely synthesizable, where the score is the percentage of heavy atoms of each new structure that ultimately appear in a retrosynthetic fragment found in the starting materials database (62-64). Furthermore, the quantum mechanics calculation helps to understand the efficiency of an atom or molecule to form different bonds based on their capacity to donate or accept electrons. The correlation between an electron and the nature of bond formation is explained by density functional theory (DFT), which is considered as a modern tool to explain quantum chemistry (65). The theorem, that is, the ground-state energy of a system of interacting electrons is a unique functionality of its electron density. This theory, first proposed by Hohenberg and Kohn (66), is the main idea of DFT (67). The ground state energy along with other molecular properties of the atoms are determined by DFT with their electronic density, providing an accurate description of the electronic structure of compounds with affordable computational cost, thus attained significant popularity in drug design application (68). The DFT optimization of designed compounds revealed that these compounds were more reactive than the parent drug, acyclovir, in which only purine ring portion served as major reactive regions. Modifications in the side chain, including the 2-hydroxyethoxymethyl improved the electrophilicity and nucleophilicity of designed compounds, which significantly enhanced hydrogen bonding interactions with receptors, as revealed from the molecular docking analysis. Indeed, modifications not only improved binding affinity but also increased binding energy. Among them, A10 showed maximum binding affinity and binding energy with polar interactions with ribocation mimics interacting residues, including Tyr88 and His257. In addition, these compounds showed optimum ADMET profile compared to that parent drug, which concludes their therapeutic capability for the treatment of T-cell mediated disease.

Conclusion

To find potent PNP inhibitors, the current study considered site-directed acyclovir modification, which was previously identified as a PNP inhibitor. Thus ten new acyclovir analogs were created by the modification of the halogen atoms and polar bulky amino group at the purine ring or side chain to improve the binding affinity towards the PNP. We, therefore, conclude that modification with a polar bulky amino group at the purine ring or side chain provides better binding affinity and increases polar interactions to PNP active sites than the incorporation of halogen atoms. All these compounds showed higher reactivity based on lower HOMO-LUMO gap with improved docking score and pharmacokinetic and pharmacodynamic properties. Among them, A10 had maximum docking score with the highest binding free energy and formed bonds with all the important residues, including His257, Tyr88. These findings help to reconsider acyclovir analogs for detailed in vitro and in vivo studies for potent inhibition of PNP to treat T-lymphocyte induced cancer and other diseases.

Conflict of interest

The authors declare no conflicts of interest.

Competing Interests

All authors declare that they have no competing interests.

References

1. Morris J, Philip E, Montgomery JA. Inhibitors of the enzyme purine nucleoside phosphorylase. Expert Opin Ther Pat 1998;8:283-99.
2. Dougados M, Amor B. Cyclosporin A in rheumatoid arthritis: preliminary clinical results of an open trial. Arthritis and rheumatolog 1987;30:83-7.
3. Weinblatt ME, Coblyn JS, Fraser PA, Anderson RJ, Spragg J, Trentham DE, et al. Cyclosporin A treatment of refractory rheumatoid arthritis. Arthritis and rheumatolog 1987;30:11-7.
4. Nickoloff BJ, Griffiths CE. Lymphocyte trafficking in psoriasis: a new perspective emphasizing the dermal dendrocyte with active dermal recruitment mediated via endothelial cells followed by intra-epidermal T-cell activation. J Clin Investig Dermatol 1990;95:S35-S7.
5. Ellis CN, Gorsulowsky DC, Hamilton TA, Billings JK, Brown MD, Headington JT, et al. Cyclosporine improves psoriasis in a double-blind study. JAMA 1986;256:3110-6.
6. Ravandi F, Gandhi V. Novel purine nucleoside analogues for T-cell-lineage acute lymphoblastic leukaemia and lymphoma. Expert Opin Investig Drugs 2006;15:1601-13.
7. Wise DS, Shewach DS, Daddona PE, Townsend LB. Certain 8-Amino-9-(benzyl) guanines as potential purine nucleoside phosphorylase inhibitors. Eur J Med Chem 1994;29:3-9.
8. Alangari A, Al-Harbi A, Al-Ghonaium A, Santisteban I, Hershfield M. Purine nucleoside phosphorylase deficiency in two unrelated Saudi patients. Ann Saudi Med 2009;29:309-12.
9. Hiddemann W, Büchner T, Wörmann B, Ritter J, Creutzig U, Plunkett W. Acute Leukemias VII: Experimental Approaches and Novel Therapies: Springer Science and Business Media 2012.
10. Markert ML. Purine nucleoside phosphorylase deficiency. Immunodefic Rev 1991;3:45-81.
11. Georgiev VS. Enzymes of the purine metabolism: inhibition and therapeutic potential. Ann NY Acad Sci 1993;685:207-16.
12. Montgomery JA. Purine nucleoside phosphorylase: a target for drug design. Med Res Rev 1993;13:209-28.
13. Seley-Radtke KL, Yates MK. The evolution of nucleoside analogue antivirals: A review for chemists and non-chemists. Part 1: Early structural modifications to the nucleoside scaffold. Antiviral Res 2018;154:66-86.
14. Tuttle JV, Krenitsky TA, Elion GB. Effects of acyclovir and its metabolites on hypoxanthine-guanine phosphoribosyltransferase. Biochem Pharmacol 1983;32:3011-5.
15. Raha K, Peters MB, Wang B, Yu N, Wollacott AM, Westerhoff LM, et al. The role of quantum mechanics in structure-based drug design. Drug Discov Today 2007;12:725-31.
16. Wang E, Sun H, Wang J, Wang Z, Liu H, Zhang JZ, et al. End-Point Binding Free Energy Calculation with MM/PBSA and MM/GBSA: Strategies and Applications in Drug Design. Chem Rev 2019;119: 9478-508.
17. dos Santos DM, Canduri F, Pereira JH, Dias MV, Silva RG, Mendes MA, et al. Crystal structure of human purine nucleoside phosphorylase complexed with acyclovir. Biochem Biophys Res Commun 2003;308:553-9.
18. Case DA, Darden T, Cheatham T, Simmerling CL, Wang J, Duke RE, et al. Amber 10. University of California, 2008.
19. Dash R, Emran TB, Uddin MMN, Islam A, Junaid M. Molecular docking of fisetin with AD associated AChE, ABAD and BACE1 proteins. Bioinformation 2014;10:562-8.
20. Dash R, Hosen SZ, Sultana T, Junaid M, Majumder M, Ishat IA, et al. Computational Analysis and Binding Site Identification of Type III Secretion System ATPase from Pseudomonas aeruginosa. Interdiscip Sci 2016;8:403-11.
21. Hosen SZ, Dash R, Khatun M, Akter R, Bhuiyan MHR, Rezaul M, et al. In silico ADME/T and 3D QSAR analysis of KDR inhibitors. J Appl Pharm Sci 2017;7:120-8.
22. Becke AD. Density-functional thermochemistry. III. The role of exact exchange. J Chem Phys 1993;98:5648-52.
23. Lee C, Yang W, Parr RG. Development of the Colle-Salvetti correlation-energy formula into a functional of the electron density. Phys Rev B Condens Matter 1988 ;37:785-89.
24. Tripathi SK, Singh SK. Insights into the structural basis of 3,5-diaminoindazoles as CDK2 inhibitors: prediction of binding modes and potency by QM-MM interaction, MESP and MD simulation. Mol bioSyst 2014;10:2189-201.
25. Pietro WJ, Hehre WJ. Molecular orbital theory of the properties of inorganic and organometallic compounds. 3. STO-3G basis sets for first-and second-row transition metals. J Comput Chem 1983;4:241-51.
26. Binkley JS, Pople JA, Hehre WJ. Self-consistent molecular orbital methods. 21. Small split-valence basis sets for first-row elements. J Am Chem Soc 1980;102:939-47.
27. Bochevarov AD, Harder E, Hughes TF, Greenwood JR, Braden DA, Philipp DM, et al. Jaguar: A high performance quantum chemistry software program with strengths in life and materials sciences. Int J Quantum Chem 2013;113:2110-42.
28. Dash R, Junaid M, Islam N, Akash C, Forhad M, Khan M, et al. Molecular insight and binding pattern analysis of Shikonin as a potential VEGFR-2 inhibitor. Curr Enzyme Inhib 2017;13:235-44.
29. Hosen SZ, Rubayed M, Dash R, Junaid M, Mitra S, Alam MS, et al. Prospecting and Structural Insight into the Binding of Novel Plant-Derived Molecules of Leea indica as Inhibitors of BACE1. Curr Pharm Des 2018;24:3972-9.
30. Junaid M, Dash R, Islam N, Chowdhury J, Alam MJ, Nath SD, et al. Molecular simulation studies of 3, 3′-Diindolylmethane as a Potent MicroRNA-21 Antagonist. J Pharm Bioallied Sci 2017;9:259-65.
31. Elhenawy AA, Al-Harbi L, Moustafa GO, El-Gazzar M, Abdel-Rahman RF, Salim AE. Synthesis, comparative docking, and pharmacological activity of naproxen amino acid derivatives as possible anti-inflammatory and analgesic agents. Drug Des Devel Ther 2019;13:1773-90.
32. Labute P. The generalized Born/volume integral implicit solvent model: estimation of the free energy of hydration using London dispersion instead of atomic surface area. J Comput Chem 2008;29:1693-8.

33. Dash R, Mitra S, Arifuzzaman M, Hosen SZ. In silico quest of selective naphthyl-based CREBBP bromodomain inhibitor. In Silico Pharmacol 2018;6:1.

34. Mitra S, Dash R. Structural dynamics and quantum mechanical aspects of shikonin derivatives as CREBBP Bromodomain inhibitors. J Mol Graph Model 2018;83:42-52.

35. Dash R, Hosen SZ, Karim MR, Kabir MSH, Hossain MM, Junaid M, et al. In silico analysis of indole-3-carbinol and its metabolite DIM as EGFR tyrosine kinase inhibitors in platinum resistant ovarian cancer vis a vis ADME/T property analysis. J Appl Pharm Sci 2015;5:73-8.

36. Dash R , Hosen SMZ, Rahman MG, Emran TB, Uddin MMN. Evolution of selective COX-2 inhibitor from Alangium salvifolium: an in silico approach. J Appl Pharm Sci 2015;5:89-93.

37. Yang H, Lou C, Sun L, Li J, Cai Y, Wang Z, et al. admetSAR 2.0: web-service for prediction and optimization of chemical ADMET properties. Bioinformatics 2018;35:1067-9.

38. Stein JM, Stoeckler JD, Shih-Ying L, Tolman RL, MacCoss M, Anna C, et al. Inhibition of human purine nucleoside phosphorylase by acyclic nucleosides and nucleotides. Biochem Pharmacol 1987;36:1237-44.

39. Omura GA. Inhibitors of the enzyme purine nucleoside phosphorylase as potential therapy for psoriasis. Curr Pharm Des 2000 Jun 1;6:943-59.

40. Ho M-C, Shi W, Rinaldo-Matthis A, Tyler PC, Evans GB, Clinch K, et al. Four generations of transition-state analogues for human purine nucleoside phosphorylase. Proc Natl Acad Sci USA 2010;107:4805-12.

41. Nunez S, Wing C, Antoniou D, Schramm VL, Schwartz SD. Insight into catalytically relevant correlated motions in human purine nucleoside phosphorylase. J Phys Chem A 2006;110:463-72.

42. Ealick SE, Babu YS, Bugg CE, Erion MD, Guida WC, Montgomery JA, et al. Application of crystallographic and modeling methods in the design of purine nucleoside phosphorylase inhibitors. Proc Natl Acad Sci USA 1991;88:11540-4.

43. de Azevedo Jr WF, Canduri F, dos Santos DM, Pereira JH, Dias MVB, Silva RG, et al. Crystal structure of human PNP complexed with guanine. Biochem Biophys Res Commun 2003;312:767-72.

44. Canduri F, dos Santos DM, Silva RG, Mendes MA, Basso LA, Palma MS, et al. Structures of human purine nucleoside phosphorylase complexed with inosine and ddI. Biochem Biophys Res Commun 2004;313:907-14.

45. Bzowska A, Kulikowska E, Shugar D. Linear free energy relationships for N (7)-substituted guanosines as substrates of calf spleen purine nucleoside phosphorylase. Possible role of N (7)-protonation as an intermediary in phosphorolysis. Z Naturforsch C 1993;48:803-11.

46. Ghanem M, Murkin AS, Schramm VL. Ribocation transition state capture and rebound in human purine nucleoside phosphorylase. Chem Biol 2009;16:971-9.

47. Tripathy S, Sahu SK. In-silico studies on Molecular Orbital's, Geometry Optimization and Molecular Docking of Curcumin as an antibacterial drug targets FtsZ protein. J Peer Sci 2018;1:e1000006.

48. Han W, Zhu J, Wang S, Xu D. Understanding the phosphorylation mechanism by using quantum chemical calculations and molecular dynamics simulations. J Phys Chem B 2016;121:3565-73.

49. Dash R, Arifuzzaman M, Mitra S, Abdul MH, Absar N, Hosen SMZ. Unveiling the Structural Insights into the Selective Inhibition of Protein Kinase D1. Curr Pharm Des 2019;25:1059-74.

50. Obot IB, Obi-Egbedi NO, Umoren SA, Ebenso EE. Synergistic and antagonistic effects of anions and Ipomoea invulcrata as green corrosion inhibitor for aluminium dissolution in acidic medium. Int J Electrochem Sci 2010;5:994-1007.

51. Dar AM, Mir S. Molecular docking: approaches, types, applications and basic challenges. J Anal Bioanal Tech 2017;8:1-7.

52. Selick HE, Beresford AP, Tarbit MH. The emerging importance of predictive ADME simulation in drug discovery. Drug Dis Today 2002 ;7:109-16.

53. Carpenter TS, Kirshner DA, Lau EY, Wong SE, Nilmeier JP, Lightstone FC. A method to predict blood-brain barrier permeability of drug-like compounds using molecular dynamics simulations. Biophys J 2014;107:630-41.

54. Guengerich FP. Cytochrome P-450 3A4: regulation and role in drug metabolism. Annu Rev Pharmacol Toxicol 1999;39:1-7.

55. Ekins S, Crumb WJ, Sarazan RD, Wikel JH, Wrighton SA. Three-dimensional quantitative structure-activity relationship for inhibition of human ether-a-go-go-related gene potassium channel. J Pharmacol Exp Ther 2002;301:427-34.

56. Evans GB, Schramm VL, Tyler PC. The transition to magic bullets–transition state analogue drug design. Med Chem Comm 2018;9:1983-93.

57. Gebre ST, Cameron SA, Li L, Babu YS, Schramm VL. Intracellular rebinding of transition-state analogues provides extended in vivo inhibition lifetimes on human purine nucleoside phosphorylase. Jo Biolog Chem 2017;292:15907-15.

58. Ayala-Fontánez N, Soler DC, McCormick TS. Current knowledge on psoriasis and autoimmune diseases. Psoriasis (Auckl) 2016;6:7-32.

59. Rose NR. Autoimmune diseases. International Encyclopedia of Public Health: Elsevier Inc 2008:267-71.

60. Gandhi V, Kilpatrick JM, Plunkett W, Ayres M, Harman L, Du M, et al. A proof-of-principle pharmacokinetic, pharmacodynamic, and clinical study with purine nucleoside phosphorylase inhibitor immucillin-H (BCX-1777, forodesine). Blood 2005;106:4253-60.

61. Schramm VL. Enzymatic transition state theory and transition state analogue design. J Biol Chem 2007;282:28297-300.

62. Baber J, Feher M. Predicting synthetic accessibility: application in drug discovery and development. Mini Rev Med Chem 2004;4:681-92.

63. Podolyan Y, Walters MA, Karypis G. Assessing synthetic accessibility of chemical compounds using machine learning methods. J Chem Inf Model 2010;50:979-91.

64. Ertl P, Schuffenhauer A. Estimation of synthetic accessibility score of drug-like molecules based on molecular complexity and fragment contributions. J Chemnform 2009;1:8.

65. Zhan C-G, Nichols JA, Dixon DA. Ionization potential, electron affinity, electronegativity, hardness, and electron excitation energy: molecular properties from density functional theory orbital energies. J Phys Chem A 2003;107:4184-95.

66. Hohenberg P, Kohn W. Physical Rev 136. B864. 1964.

67. Car R. Introduction to Density Functional Theory and ab Initio Molecular Dynamics. QSAR 2002;21:97-104.

68. Shenna ML, Donald FW. A Review of Density Functional Theory Quantum Mechanics as Applied to Pharmaceutically Relevant Systems. Curr Comput-Aid Drug Des 2007;3:290-6.